ENHANCEMENT OF FOG-COLLECTION EFFICIENCY OF A RASCHEL MESH USING SURFACE COATINGS AND GEOMETRIC CHANGES

by

MITHUN RAJARAM

Presented to the Faculty of the Graduate School of

The University of Texas at Arlington in Partial Fulfillment

of the Requirements

for the Degree of

MASTER OF SCIENCE IN MECHANICAL ENGINEERING

THE UNIVERSITY OF TEXAS AT ARLINGTON

December 2015

Acknowledgements

Words cannot be framed to convey my deepest gratitude and respect for my thesis advisor and committee chair, Professor Cheng Luo. His expertise in the field Micro/ Nano system, excellent guidance, patience motivated me to become an independent researcher and I am grateful for providing me with an excellent atmosphere for doing research. Till this date I have never seen a hardworking person like him and he is my biggest inspiration and he always inspired me with innovative thoughts. I would like to extend my deepest gratitude to Dr. Xin Heng, who helped me in his busy schedule to make me understand the basic process and being gentle to explain the concepts in detail. His nature of helping people and time management skill helped me to understand the importance of time and to accomplish all my works precisely on time. I want to thank my thesis committee member Dr. Hyejin Moon and Dr. Zhen Xue Han, who took time to be on the committee and to guide me. I have been amazingly fortunate enough to work with you all.

I want to thank all the staffs at CCMB, Nanofab Research Centre and Fablab for the training and helping me in fabrication and image sensing processes. I would also like to acknowledge the support of my group members Mr. Bharathram Vishweswaran, Mr. Manjarik Mrinal and all other colleagues during the progress of my thesis.

I want to thank my family, my mom, my dad, my brother and my grandparents for their endless love and for constantly motivating me to bring the best out of me. I would also like to remember my late grandmother whose blessings are always with me.

I want to thank Mr. Gowtham Subramanian, Mr. Hariram Baskar, Mr. Kaushik Narayan and all my friends who were all with me through thick and thin.

Finally, I would like to dedicate this thesis to my father, Mr. Rajaram, my mother, Mrs. Kaliyammal and to my best friend Nivetha for their endless patience, motivation and the countless sacrifices they made for providing me the best educational opportunities and this work was not possible without their constant love and encouragement.

November 23, 2015

Abstract

ENHANCEMENT OF FOG-COLLECTION EFFICIENCY OF A RASCHEL MESH USING SURFACE COATINGS AND GEOMETRIC CHANGES

Mithun Rajaram, MS

The University of Texas at Arlington, 2015

Supervising Professor: Cheng Luo

In a few countries, such as Chile, a Raschel mesh is widely used in the field to collect fog. In this work, we explored the possibility of enhancing fog-collection efficiency of a typical Raschel mesh through surface modification and geometric changes. We demonstrated about 100% enhancement in the fog-collection efficiency.

Table of Contents

List of Illustrations

List of Tables

Chapter 1

Introduction

In addition to energy, the issue of water shortage and scarcity is one of major global concerns, since about one billion people living in rural areas of African, Asian, and Latin American countries do not have access to clean water sources [1]. A water shortage has been a major problem faced by the modern civilization in both arid and humid environment [2]. In the case of deserts and semi-deserts, which occupy 50% of the Earth's land area, the most precipitation is in the form of dew [3], which is the main water source to, e.g., cacti [4], beetles [5,6], dune grasses [7] and cotula fallax plants [8]. Furthermore, in an arid environment with little rainfall every year, fog and dew may always exist when temperature is deceased in late nights and early mornings. Several artificial fog collectors have been developed, which mostly mimicked the fog-collection mechanisms of desert animals and plants [5,4,9-16]. However, these collectors appear still at the stage of laboratory research, and have not yet been applied in the field.

For the last two decades, in at least five countries, such as Chile, the most commonly used large fog collector in the field employs a Raschel mesh that is vertically oriented between two poles to collect water from fog and dew [17, 18, 19]. The Raschel mesh has meter-scaled lengths and widths (Fig. 1(a)). It also has mm-scaled pores and filaments. The pores have approximately triangular shapes, and some filaments are inclined with lengths close to 1 cm (Fig. 1(b)). The filaments are about 20 μm thick, while their joints are 0.2 to 0.4 mm thick.

The fog collection of a Raschel mesh includes two steps. Water vapors are first condensed on filaments. Under gravity, large condensed drops then drain off from the filaments to an underneath gutter. Raschel meshes are effective in fog collection. Their fog collection rates are typically 1-10 L/m2 per day [20]. Also, the presence of light rain with the fog has produced collection rates as high as 300 L/m2 per day for a wind speed of 10 m/s [20].

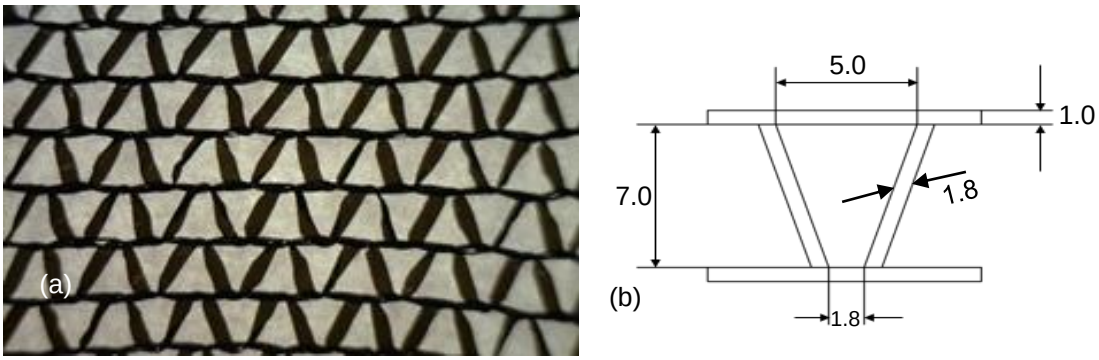

Figure 1: (a) Front view of part of a Raschel mesh, and (b) Dimensions of its pores and the filament (unit: mm)

On the other hand, there is still a large room to improve their fog-collection efficiency. According to recent experimental results, only around 2% of water vapors that pass by a typical Raschel mesh have been collected by this mesh [13]. In contrast, an optimal mesh with rectangular pores has shown a five-time enhancement in the fog-collection efficiency of a typical Raschel mesh. Meanwhile, it has already been demonstrated that Raschel meshes are effective in the field to harvest water. Thus, a Raschel mesh should have its unique advantages in collecting water from fog.

Using woven olefin Raschel meshes (Fig. 1), Schemenauer, Cereceda, and their co-workers have conducted numerous pilot-scale studies that demonstrate the feasibility of harvesting fog [21-24]. However, as commented in [13], most studies on mesh-based fog harvesters have been performed in the field using uncontrolled natural fog conditions, and systematic studies of these fog harvesters under laboratory conditions have been rare [19,21-27]. Thus, in this work, we explore a Raschel mesh under laboratory conditions for the purpose of optimizing the Raschel mesh.

Chapter 2

Theoretical Background and Comparison Tests

2.1. Theoretical Background

The collection efficiency, η, of a mesh depends on aerodynamic collection efficiency (η_{ace}), capture efficiency (η_{cap}), and draining efficiency (η_{dra}) [28]:

$$\eta = \eta_{ace}\, \eta_{cap}\, \eta_{dra}. \quad (1)$$

All of these three efficiencies are not larger than 100%. η_{ace} is the fraction of the unperturbed water flux heading towards a mesh that would collide with the mesh filaments. η_{cap} is the fraction of the collided water vapors that actually deposit on filaments from the fog flow initially headed toward the filaments. η_{dra} is the fraction of the deposited water that would drain off from the filament, which is subsequently collected through a gutter located at the bottom of the mesh.

The possibility of improving η_{ace} of a Raschel mesh has been previously considered by other researchers [13]. η_{ace} is related to shade coefficient (SC), which is the ratio of the filament area over the total mesh area. η_{ace} does not necessarily increase with the decrease in the pore area. In terms of a theoretical model derived in [13], η_{ace} is only 9% for a solid plate, which has no pores. It is 20% for a typical Raschel mesh, whose SC is 35 to 37%. However, η_{ace} can be easily improved to the maximum value of 24.5% if SC is 55%, when the filament area of a typical Raschel mesh is increased relative to the pore area.

Langmuir and Blodgett have previously derived an empirical expression of η_{cap} for a circular cylinder [29]. This expression, together with the theoretical model of [22], was adopted in [13] to optimally design rectangular meshes, which have circular filaments. Since the filaments of a Raschel mesh have rectangular cross-sections, instead of circular ones, the empirical expression of η_{cap} may not be applicable to the Raschel mesh. In addition, we have not seen any theoretical models for η_{dra}. Thus, we would like to have a good understanding about these two efficiencies through experiments.

2.2 Comparison Tests

Fog-collection experiments were performed on different meshes using an experimental setup shown in Fig. 2. Each test is conducted at room temperature (24°C ± 1°C). Two humidifiers (models: EE- 5301, Crane USA Co., and AOS 7135 Ultrasonic, BONECO USA Co.) are connected to generate the mist flow. A plastic pipe is employed to guide this mist flow. A fan (model: Breeze color USB Desktop fan, Arctic USA Co.) is used at 800 rounds per minute to increase the mist flow speed. At the end of the pipe, the mist flow speed is 1.1 m/s, which is measured using a wind speed meter (model: WM- 2 Handheld Weather meter, AmbientWeather USA Co.). The entire process is conducted in a closed chamber. 100% humidity is maintained inside the chamber and a humidity meter (model: Hydro- Thermometer Humidity Alert with Dew Point- 445815, EXTECH USA Co.) is used to monitor the humidity throughout a process cycle. A tested mesh is placed 5 cm away from the exit of the pipe, and a glass container is put below the mesh to collect water that drains down.

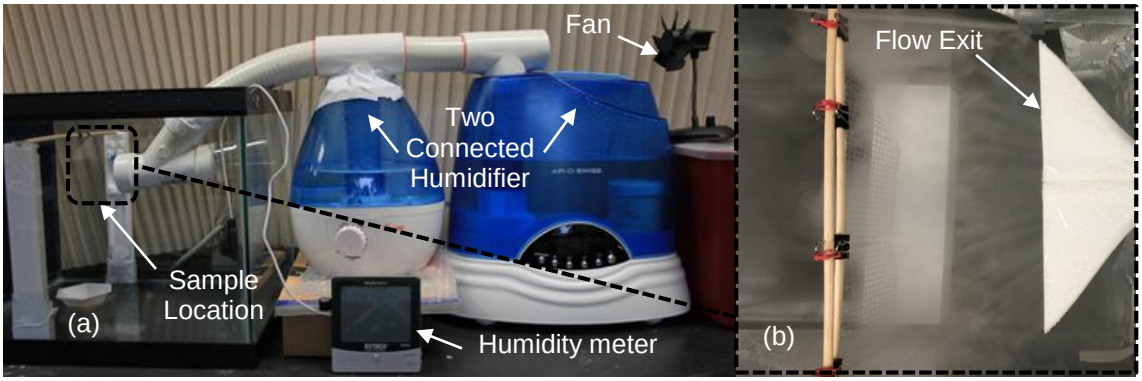

Figure 2: (a) Experimental setup for the water collection and (b) Flow exit and location of sample.

Two rectangular meshes and a typical Raschel mesh were initially tested (Fig. 3). The two rectangular meshes have a main draining path different from that of the Raschel mesh. In the case of these rectangular meshes, every fiber has circular cross-sections. Accordingly, tiny

drops were initially seen all around a fiber, and these drops also grew along all the directions. A large drop was formed on a pore due to the coalescence of the small drops on the neighboring fibers (Fig. 3(a1)), and the large drop fell down when it was above a threshold size (Figs. 3(a1) and 3(a2)). There are two problems associated with this main draining path. First, as indicated in [18], the large drop clogs the pore area (Figs. 3(a1) and 3(a2)). This means that SC is close to 100% as in the case of a plate without any pores. Thus, η_{ace} actually decreases to the lowest value of 9% during the condensation process. Second, the drops on the side surfaces of a fiber are easily blown off by a wind, since these drops are directly exposed in the wind and lack of the support of their substrate (Fig. 3(a1)). Accordingly, this point reduces η_{dra}.

In contrast, the Raschel mesh does not have these two problems. It has rectangular fibers. Initially, tiny drops mainly appeared on the front surface of a filament, since this surface was directly exposed in the fog flow (Figs. 3(c1)). Only few drops were seen on the side surfaces of the filament. The tiny drops on the front surface of an inclined filament then merged into a large drop (Figs. 3(c1) and 3(c2)), which subsequently moved towards the joint of the filaments to coalesce with other drops at this joint (Figs. 3(c3)). During this process, due to the support of the filament surfaces and the pinning effect of the filament edges, drops were difficult to get blown off from a filament by a wind. Accordingly, almost all the water vapors that hit the filaments should be captured. Thus, the Raschel mesh should have a value of η_{cap} close to 100%.

Furthermore, the inclined filaments in a Raschel mesh, in comparison with vertical fibers in a rectangular mesh, enable drops that are located on these filaments to merge at their joint (Figs. 3(c2) and 3(c3)), increasing the rate of generating a large drop. When the drop at the joint became large enough, it overcame the adhesion force over there and fell down into the underneath water container (Figs. 3(b2) and 3(c3)). This drop did not clog much of the pore area. Therefore, in comparison with a rectangular mesh, the Raschel mesh should have a higher η_{dra}, and its η_{ace} does not decrease during the condensation process.

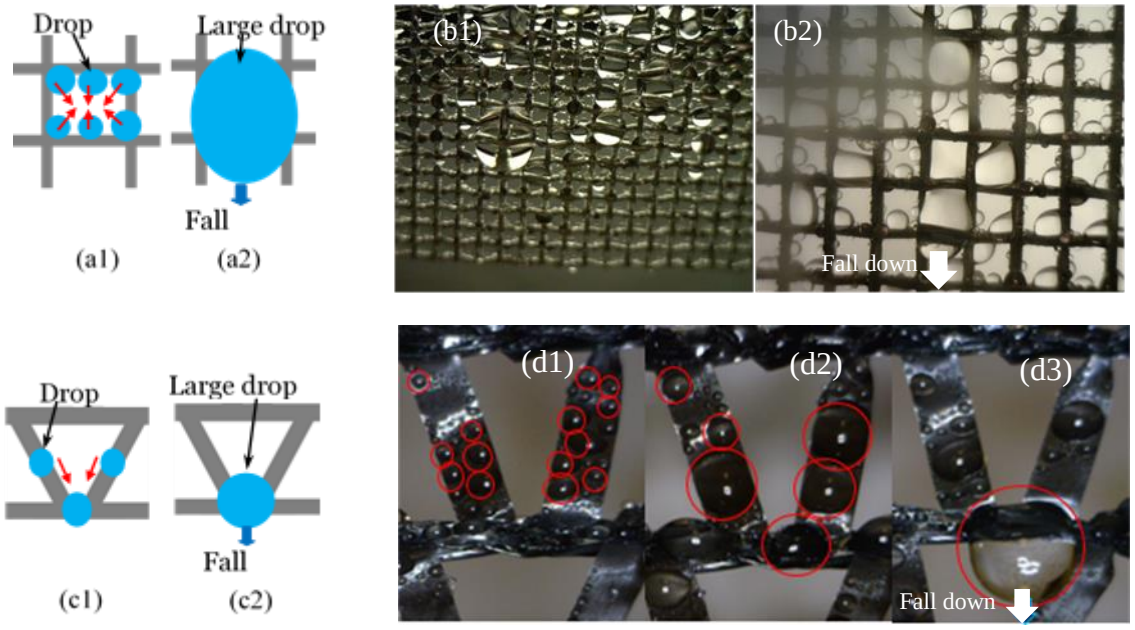

Figure 3: (a) Illustration and (b) condensation on two rectangular meshes with circular fibers. (a1) Small drops appear on the side surfaces of fibers, and (a2) these drops merge into a large one. (b1) First mesh with fiber diameter and pore spacing of 0.34 and 0.9 mm, respectively, and (b2) second mesh with fiber diameter and pore spacing of 0.89 and 2.3 mm. (c) Illustration and (d) experimental results of condensation on a Raschel mesh: (d1) small drops are condensed on the surfaces of filaments, (c1, d2) merge to form large drops, which subsequently move down to the joint of the mesh, and (c2, d3) finally detach from the joint. In (d1)-(d3), numbers denote drops, and the summation of the numbers means the corresponding drops are merged into a larger one. Scale bars represent 2 mm in (b) and 5 mm in (d).

Meanwhile, during 1-hour collection periods, the amounts of water collected by rectangular meshes I (Fig. 3(b1)) and II (Fig. 3(b2)) and the Raschel mesh, all with the same dimensions of 3.3 X 2.0 cm^2 (length X width), were 14, 17 and 16 mL, respectively. The higher collection efficiency of rectangular mesh II is considered due to that its SC is closer to the optimal value [13], resulting in a higher η_{ace}.

A discussed above, η_{cap} of the typical Raschel mesh may be considered to be approximately 100%. Therefore, in this work, we focus on increasing η_{dra} and η_{ace} of a Raschel mesh.

Chapter 3

Effects of Surface Coatings

3.1. Experimental Results

On a vertically oriented mesh, tiny drops may not be drained, because their gravity is less than the resistance force induced by the contact angle hysteresis. A coating may change wetting properties of a surface such that a tiny drop may flow down [23-25]. In this work, Teflon, ZnO nanowires, NeverWet, and hydrobead were, respectively, coated on Raschel meshes to examine their effects on increasing η_{dra}. The corresponding meshes were, respectively, referred to as “Teflon mesh,” “nanowire mesh,” “NeverWet mesh,” and “Hydrobead mesh.” These four meshes, together with as-received Raschel meshes, were tested. As in the previous tests, all the tested samples had the same dimensions of 3.3 cm X 2.0 cm. The coatings are relatively easy to generate on Raschel meshes. Both NeverWet and hydrobead are commercially available, and they are often applied to enhance surface hydrophobicity. Both of them were spray-coated on meshes, while Teflon was dip-coated. ZnO nanowires were grown on the meshes using a hydrothermal approach [33].

Figure 4 shows surface structures on the coated meshes. The nanowires had hexagonal cross-sections with an average length of 2.1 μm, diameter of 0.36 μm and distance of 0.36 μm (Fig. 4a). They have different orientations and their tips are close to each other. Both of NeverWet and hydrobead have cracks in their coatings. The NeverWet coating has a thickness of 2.2 μm. The cracks are linked with each other, and have widths less than 10 μm (Fig. 4b). Also, the distance between two neighboring cracks is usually above 100 μm. The hydrobead coating is about 1.8 μm thick. The widths of the cracks range from 1 to 40 μm, and their lengths vary from 10 to 180 μm (Fig. 4c). Most of the cracks have widths and lengths of around 15 and 100 μm, respectively. The distances between the cracks range from 20 μm to 200 μm. The receding and advancing contact angles were measured on the five meshes. The measurement has an error of 2^o. The receding contact angles of Raschel, Teflon, NeverWet, Hydrobead and nanowire meshes were measured to be 98^o, 120^o, 154^o, 156^o and 112^o,

respectively. The corresponding advancing contact angles were measured to be 113^{o}, 125^{o}, 156^{o}, 158^{o}, 138^{o}. The contact hystereses are 15^{o}, 5°, 2°, 2°, and 26**°**, respectively. After 1-hour durations, Teflon, NeverWet, hydrobead and ZnO nanowires meshes collected 14, 16, 17 and 13 mL of water, respectively, whereas the as-received Raschel mesh collected only 11 mL. Therefore, the hydrobead has shown the highest collection efficiency, which is about 1.55 times that of the as-received Rashel mesh.

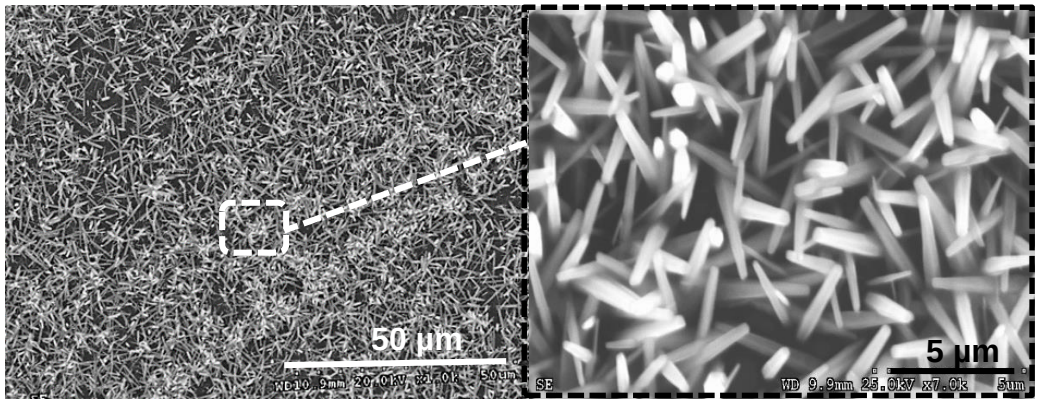

(a1) (a2)

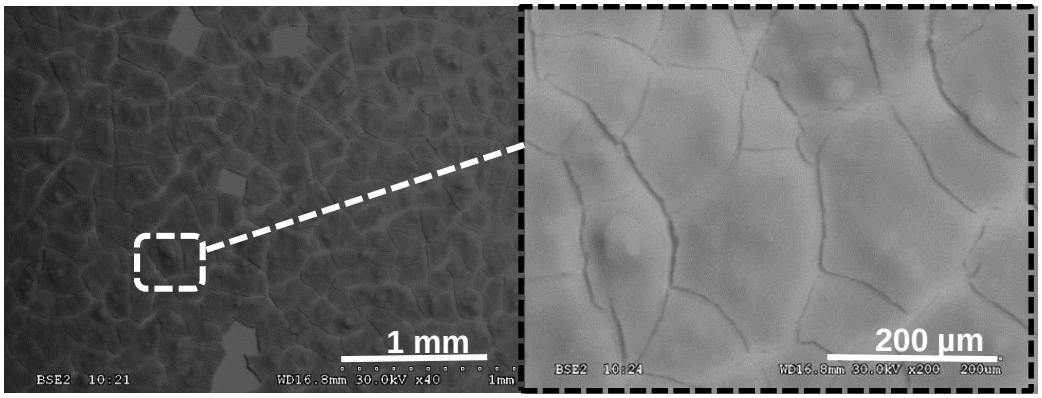

(b1) (b2)

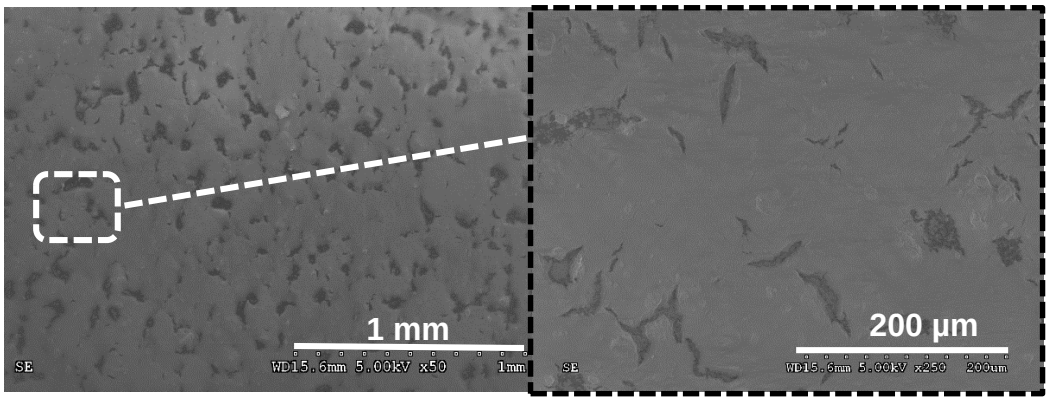

(c1) (c2)

Figure 4: Top (SEM) views of the coatings: (a) ZnO nanowires, (b) NeverWet, and (c) hydrobead.

3.2. Simple Model

A simple model is developed to explain the fog-collection results on different coatings. Due to gravity, large drops that are condensed on a mesh may move down from the mesh. However, tiny drops may get stuck on the filaments and thus are not harvested. Hence, to enhance collection efficiency, it is important to harvest these tiny drops as much as possible. A simple model is developed for this purpose. Let θ denote apparent contact angle of the drop. If the substrate is smooth, then θ is intrinsic contact angle. A liquid drop on a substrate that is inclined by an angle of β suffers a gravitational force G and a threshold adhesive force F. The two forces, respectively, have the following expressions:

$$G=\rho g V \sin\beta , \tag{2}$$

$$F = AF_o , \tag{3}$$

where ρ denotes mass density of the liquid, g is gravitational acceleration, V is the volume of the drop, A is the area of the drop base, and F_o is the adhesive force per unit area of the drop base. If

$$G \geq F , \tag{4}$$

the drop moves down from the substrate. The contact area between a drop and its substrate increases with increasing θ. That is, for a drop with a fixed V, A decreases with the increase in θ. Therefore, for a tiny drop to move, by Relations (2)-(4), two conditions should be met: (i) θ should be as large as possible, and (ii) F_o should be as small as possible. We desire to make the filament surface have the super-hydrophobic properties. That is, θ is greater than 150°. On a smooth surface, θ is normally less than 120°, even if this surface is coated with highly water-repellent materials [34], such as Teflon [35]. Therefore, to make the corresponding contact angle well above 120°, roughness structures are normally incorporated on a surface.

When a liquid drop is placed on a rough surface, there are two possible wetting states: Wenzel [36] or Cassie−Baxter [37]. In the Wenzel state (Fig. 5(a)), the drop completely fills grooves between roughness structures (e.g., pillars and channels), while in the Cassie−Baxter state, air is trapped between these structures and the drop stays on top of the roughness structures and trapped air. In the Cassie-Baxter state, the drop stays on top of the roughness structures, which reduces its contact area with the substrate and makes it easy to roll off from the substrate. In the Wenzel state, although θ may still be large, the roughness structures may pin the drop, making it difficult to move off from the surface. It has been reported, for example, in [38,39] that, during the condensation process, water vapor penetrated into the surface roughness grooves [38,39], causing the pinning of a drop on a lotus leaf. Such results imply that, during the condensation process, the wetting is normally in the Wenzel state. Our focus now is thus on reducing the pinning effect in the Wenzel state.

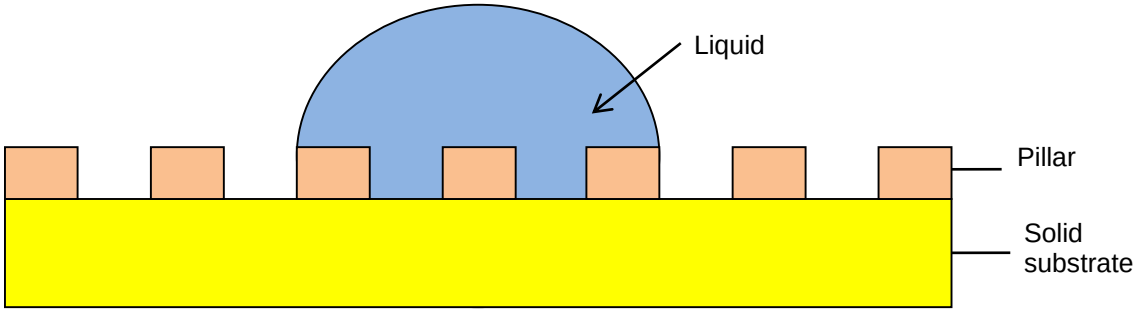

(a)

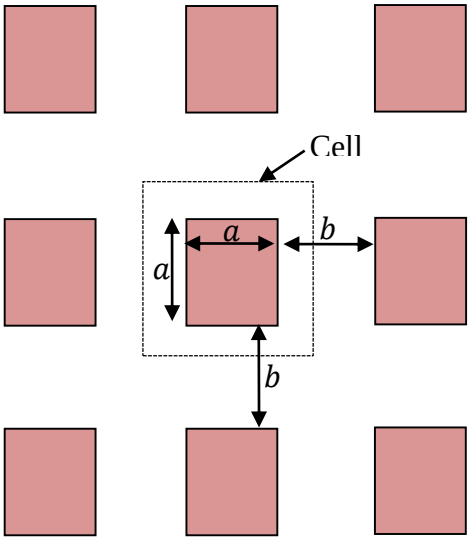

(b)

Figure 5: (a) Schematic side view of Wenzel state, and (b) schematic top view of an array of square micropillars.

Let θ_0 denote intrinsic contact angle. The Wenzel equation for Wenzel state is [29]:

$$\cos\theta = r\cos\theta_0. \tag{5}$$

In this equation, r denotes the roughness ratio. It is the ratio of the actual surface area of the rough surface, A_a, to the projected surface area, A_p, and is given by

$$r = \frac{A_a}{A_p}. \tag{6}$$

It is observed from this equation that

$$r \geq 1. \tag{7}$$

When r is 1, it implies that the surface is smooth. As observed from Relations (5) and (7), to make θ larger than θ_0, θ_0 should be larger than 90°, indicating that the surface coating should be hydrophobic.

To have a good understanding about r for choosing it properly, consider a regular squared micropillar array with a pillar size of *a X a*, spacing of *b*, and height of *h*, which is a type of simple structures. Considering a representative cell around a micropillar (Fig. 5(b)), we have $A_p = (a+b)^2$ and $A_a = 4ah + (a+b)^2$, where A_a actually equals the addition of A_p with the four pillar sidewall areas. By Eq. (6), the corresponding r is

$$r = 1 + \frac{4ah}{(a+b)^2}. \tag{8}$$

It can be seen from this equation that, for given *a*, *r* increases with the increase in *h* and decrease in *b*.

Next, let's consider two special cases. In the first case, we assume that *b*<<*a*. Accordingly, we get

$$r \approx 1 + \frac{4h}{a}. \tag{9}$$

Subsequently, given that θ_0 =100°, by Eqs. (5) and (9), to make θ equal 150°, we should have $h = a$. In the second case, we assume that *b*=*a*. Given that θ_0 =100°, by Eq. (9), we should have *h*=5*a* to get θ =150°. The surface structures in the two cases are illustrated in Fig. 6. Two points can be observed. First, there are narrow gaps between the structures in Case I (Fig. 6(a)), while such gaps are relatively wide in Case II (Fig. 6(b)). Second, the height/width ratios of the structures in these two cases are 1 and 5, respectively. These two differences indicate that, although the structures in the two surfaces produce the same r, which also resulted in the same A, the values of F_o are different. In Case II, the pillars penetrate a water drop, and the sidewalls of these structures block the movement of the drop. In contrast, in Case I, the water in narrow gaps can be considered stationary, and it becomes part of the substrate surface. The portion of the drop located above the substrate moves on this composite substrate surface (Fig. 6(a)). Accordingly, the drop in Case I should suffer a smaller F_o than that in Case II.

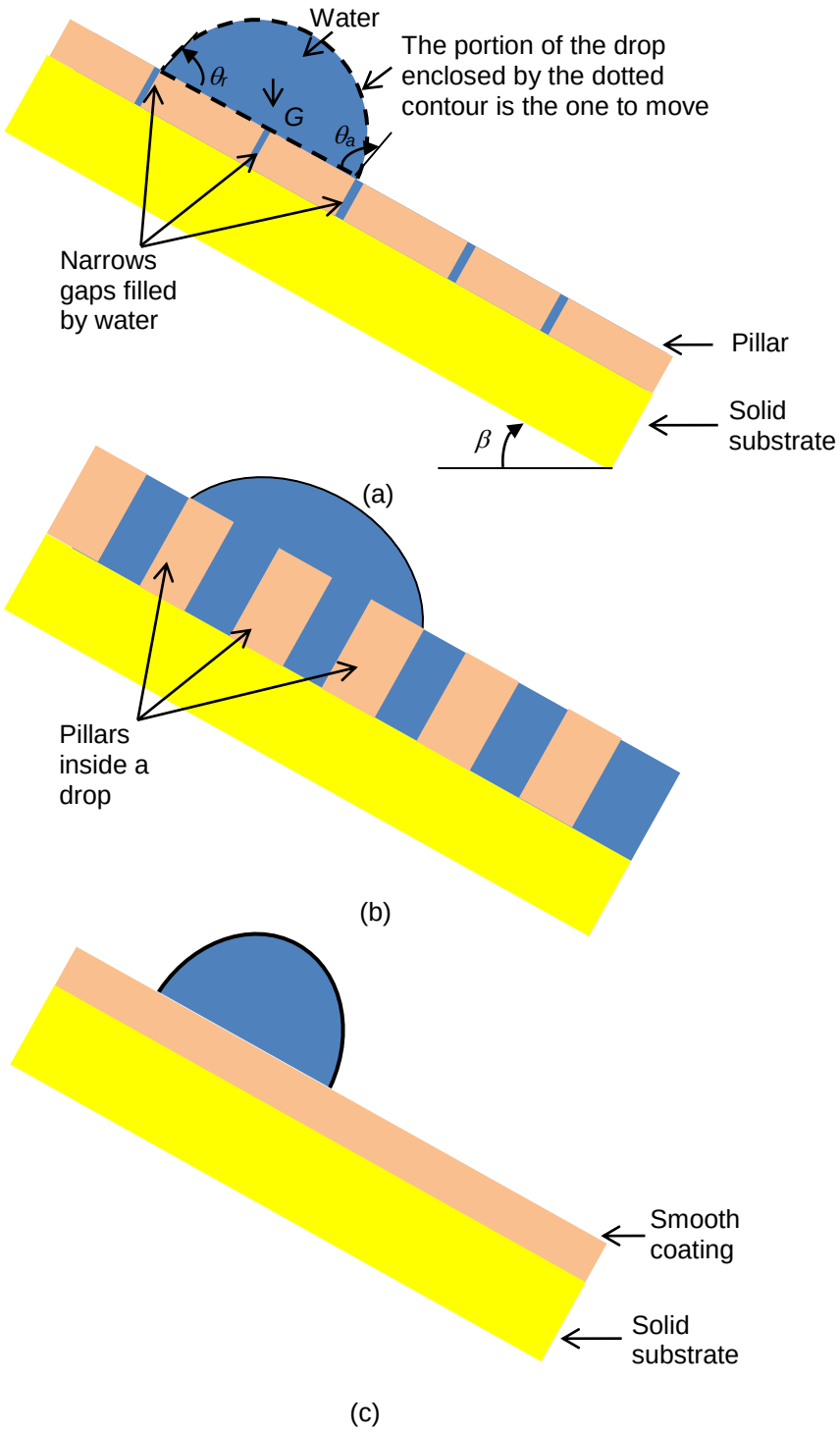

Figure 6: Two wetting situations in Wenzel wetting state: (a) low aspect-ratio structures with narrow gaps, and (b) high aspect-ratio structures with wide gaps. (c) Wetting on a flat surface.

Furthermore, the drop volume is in the order of the third power of its radius. Since *b*<<*a*, it is readily shown the total gap sizes are much smaller than the drop radius. This result indicates that, as far as the volume is concerned, that the amount of water inside the narrow gaps can be neglected in comparison with the part of the drop that moves down on the substrate.

Consider a third case, in which the substrate is flat and it is not incorporated with any roughness structures (Fig. 6(c)). In Case I, part of the solid surface in Case III is actually replaced with the surface of water that fills the narrow gaps. Accordingly, F_o in Case I is smaller than its counterpart in Case III, because the adhesion between water and solid should be larger than that between the same liquid. Furthermore, for a given drop, Case I has a smaller A than Case III due to the increase in the contact angle. Thus, *F* in Case I is smaller than that in Case III, making the corresponding drop easier to move down on the corresponding substrate. Case II also has a smaller A than Case III. However, it is not clear whether F_o also has a smaller value in Case II. Therefore, it is uncertain whether Case II has a smaller F. In summary, there are two possible results after incorporation of roughness structures. First, if the roughness structures are closer to those of Case I, then the drop is easier to move down than in Case III. Second, when these structures are closer to those of Case II, it is not clear whether the drop is easier to move down.

Let θ_r and θ_a, respectively, denote receding and advancing contact angles of the drop. θ ranges between θ_r and θ_a. The threshold adhesive force F is often expressed as

$$F = W\gamma(\cos\theta_r - \cos\theta_a) \tag{10}$$

where W is the diameter of the drop base. On the other hand, there is a problem of applying this expression to determine F. In Cases I and II, r has the same value. The same applies to θ_o. Accordingly, the resulting W should be the same in the two cases. Also, by Eq. (4),

$(\cos\theta_r - \cos\theta_a)$ should also be the same as well. Therefore, F should be the same in both cases. However, as justified above, the two cases should lead to different values of F. Hence, we consider that the use of Eq. (5) to determine $(\cos\theta_r - \cos\theta_a)$ may not be correct. Due to lack of a good approach to find it, we employ Eq. (3) instead in our model.

In our tests, the NeverWet and hydrobead belong to the first case, and ZnO nanowires the second case. According to the data given in Sub-section 3.1, the ratio of *b* with *a* for the NeverWet coating is above 10, while it is about 13 for the hydrobead. Therefore, both coatings belong to the first case, resulting in the high collection efficiency. Meanwhile, ZnO nanowires belong to the second case, and they are not as efficient as the NeverWet and hydrobead.

Chapter 4

Effects of Geometric Changes

4.1. Fabrication of the Meshes

η_{ace} of a typical Raschel mesh may be improved to the maximum value of 24.5% if SC is increased from around 36% to 55%. The existing meshes are mainly fabricated by weaving fibers together, such as a typical Raschel mesh shown in Fig. 1(a). When the same approach is used to create meshes with different SCs, there may be no polymer fibers that exactly meet the corresponding size requirements. In this work, we develop a new manufacturing method to fabricate different meshes.

To manufacture a mesh, pores have to be fabricated in a polymer sheet. Polymer or metal sheets are usually patterned after they are softened at a raised temperature using a hot-embossing process or injection molding [40]. However, it is observed that, even at room temperature, an office punch can punch holes in paper, which avoids the needs of heating and cooling a material to be patterned. Under the motivation of this observation, it should also be feasible to punch hollow patterns in a polymer sheet at room temperature.

The new method used to fabricate the desired mesh is essentially a punching process. This process uses two different rigid molds, which are, respectively, referred to as “top mold” and “bottom mold” thereafter. The top mold includes mm-scaled blocks (Fig. 7(a)). The mm-scaled blocks have sharp edges, and are employed to cut off the polymer for generating pores. The bottom mold also includes mm-scaled holes. These holes are used to assist in the cutting and removal of the cut-off polymer.

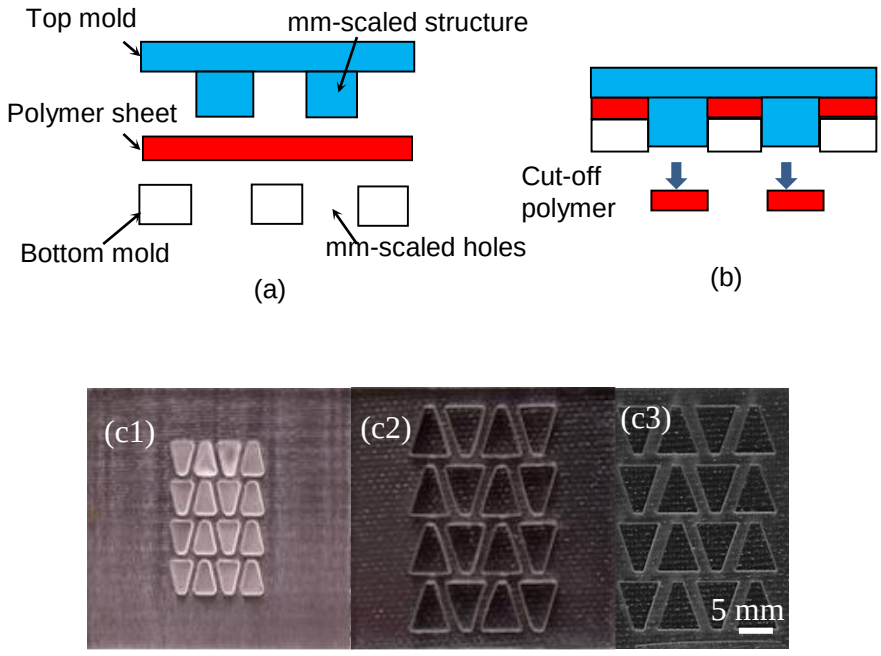

Figure 7: Two-step process to fabricate the proposed mesh (cross-sectional schematics): (a) place a polymer sheet on the bottom Al mold of the first set, and (b) at room temperature, insert the top mold into the polymer sheet to cut undesired portion of the sheet. Fabricated (c1) top and (c2) molds, and (c3) Type II PMMA mesh (optical images).

Two steps are applied in the punching process to fabricate the new mesh (Figs. 7(a) and 7(b)). First, place a polymer sheet on the bottom mold (Fig. 7(a)). Second, at room temperature, insert the top mold into the polymer sheet (Fig. 7(b)). During this step, due to the stress concentration at the sharp edge of a mm-scaled block of the top mold, the part of the polymer directly underneath this block is first cut off from the neighboring polymer, and then pushed into the corresponding hole inside the bottom mold.

The top and bottom molds were fabricated using an Epilog laser (Fig. 7(c)). With the aid of these molds, the desire meshes were generated in a poly-methyl methacrylate (PMMA) sheet using the two-step punching process. PMMA was a commonly used material in hot-embossing processes [41]. The used PMMA sheet is 30 μm thick. It is thicker than a Raschel mesh, which has a thickness of 20 μm. Three different types of PMMA meshes have been fabricated, which are called Types I, II and III meshes, respectively. As in the previous tests, the generated PMMA meshes also have the dimensions of 3.3 cm X 2.0 cm. Fig. 7(d) gives a representative Type II mesh. If needed, the molds can be applied to punch a PMMA sheet multiple times to fabricate a larger mesh. The filaments of the three types of meshes have the same widths of 1.8 mm. Type I has the same SC of 37% as a typical Raschel mesh. Types II and III have smaller pores. The distance between two inclined filaments is 1.8 mm in Type II and it is 1.0 mm in Type III. We want to examine whether the reduction in this distance could result in fast coalescence of two neighboring points at the intersection of the two filaments. The SCs for Type II and Type III are both around 51%. Accordingly, the value of η_{ace} for Type I is 21.6%, and they are both 23.3% for Type II and Type III meshes.

PMMA meshes are subsequently coated with ZnO nanowires, Teflon, and hydrobead, respectively. The NeverWet coating also has a high collection efficiency. Since its spin-coating solution etches PMMA, it is not used on the PMMA meshes.

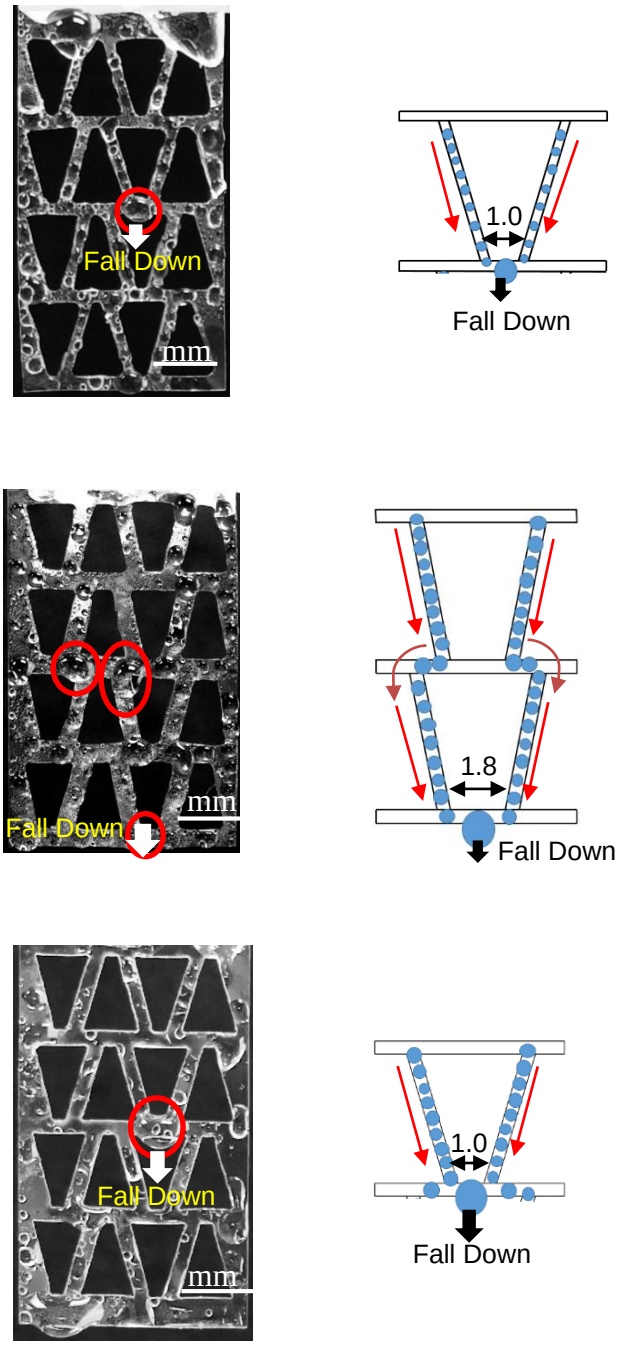

Figure 8: Different moving paths of condensed water drops on Types (a) I, (b) II, and (c) III the PMMA meshes, which are all coated with hydrobead (unit: mm).

4.2. Fog-collection Results and Discussions

Table 1 gives the amounts of water collected by the PMMA meshes. Two points are observed from this table. First, as in the previous tests, the hydrobead coating still has the highest collection efficiency among the three tested coatings in each type of meshes. Second, Types II mesh with the hydrobead coating has shown the highest collection efficiency among all the tested mesh. It has collected 23 mL water during a 1-hour period, which is 34.9 $\mu L/mm^2$. This point indicates that, with the further modification of mesh geometry, the collection efficiency has been improved from 1.55 to 2.09 times that of the as-received Rashel mesh.

Both Types II and III meshes should have higher collection efficiencies than Type I, since the former two types have higher η_{ace}. To explore why Type II mesh was more efficient in collecting fog than Type III, we explored the moving paths of condensed water drops on the meshes. As observed from Fig. 8, there are some differences in these moving paths, which influence the drop draining efficiency. The moving paths on Type I and Type III meshes are the same as that on a Raschel mesh (Fig. 3(c)). Once a large drop gets to the intersection of two inclined filaments, its growth relies on both the adsorption of the incoming water vapor and addition of new drops from the two inclined filaments. However, in Type II, a large drop moves all the way down till it is large enough to fall down from the intersection of two incline filaments. During this process, it receives additional supply of water, which is the tiny drops present on its draining path.

Table 1: Total Amount of Water Collected for 1 hr duration on different types of mesh with various coatings.

Type	Coating	Water Collected (ml)
I	ZnO	13
I	Teflon	15
I	HydroBead	18
II	ZnO	16
II	Teflon	18
II	HydroBead	23
III	ZnO	15
III	Teflon	17
III	HydroBead	21

Chapter 5

Summary and Conclusion

In this work, we explore the possibility of improving fog-collection efficiency of Raschel mesh through surface modification and geometric changes. We considered five different coatings on the mesh surfaces. Through experimental and theoretical investigations, we demonstrated that it was possible to improve the fog-collection efficiency using short roughness structures with narrow gaps. The basic idea is to increase the contact angle, while in the meanwhile reduce the pinning effect. NeverWet and HydroBead both satisfy these two requirements. As a result, their coatings have increase the collection efficiency of the Raschel mesh by about 50%, and are the most efficient among the five coatings that were tested. A new punching process was further developed to fabricate three different types of PMMA meshes. Due to the differences in SC and moving paths of condensed water drops were observed on these meshes, Type II meshes have shown another 50% enhancement in fog-collection efficiency.

References

1. *Progress on Sanitation and Drinking Water*: *2010 Update*. World Health Organization: Geneva, (2010).
2. (a) Rosegrant, M.W.; Cai, X.; Cline, S.A. *Global Water Outlook to 2025: Averting an Impending Crisis*; International Food Policy Research Institute: Washington, DC, 2002. (b) Shiklomanov, I. A. Appraisal and assessment of world water resources. *Water international*, Vol. 25, 11-32 (2000).
3. Middleton, N. *Deserts: A Very Short Introduction*. Oxford University Press, New York, pp. 4, 16, and 19 (2009).
4. Ju, J.; Bai, H.; Zheng, Y.; Zhao, T.; Fang, R.; Jiang, L. A multi-structural and multi-functional integrated fog collection system in cactus. *Nature communications*, Vol. 3, 1247 (2012).
5. Parker, A. R.; Lawrence, C. R. Water capture by a desert beetle. *Nature*, Vol. 414, 33-34 (2001).
6. Nørgaard, T.; Dacke, M. Fog-basking behaviour and water collection efficiency in Namib Desert Darkling beetles. *Frontiers in zoology*, Vol. 7, 23 (2010).
7. Ebner, M.; Miranda, T.; Roth-Nebelsick, A. Efficient fog harvesting by Stipagrostis sabulicola (Namib dune bushman grass). *Journal of Arid Environments*, Vol. 75, 524-531 (2011).
8. Andrews, H. G.; Eccles, E. A.; Schofield, W. C. E.; Badyal, J. P. S. Three-Dimensional Hierarchical Structures for Fog Harvesting. *Langmuir*, Vol. 27, 3798-3802 (2011).
9. Zhai, L.; Berg, M. C.; Cebeci, F. C.; Kim, Y.; Milwid, J. M.; Rubner, M. F.; Cohen, R. E. Patterned Superhydrophobic Surfaces: Toward a Synthetic Mimic of the Namib Desert Beetle *Nano Lett.* 2006, *6*, 1213-1217.

10. Garrod, R.; Harris, L.; Schofield, W.; McGettrick, J.; Ward, L.; Teare, D.; Badyal, J. Mimicking a Stenocara Beetle's Back for Microcondensation Using Plasmachemical Patterned Superhydrophobic-superhydrophilic Surfaces *Langmuir* 2007, *23*, 689-693.
11. Dorrer, C.; Rühe, J. R. Mimicking the Stenocara Beetle Dewetting of Drops from a Patterned Superhydrophobic Surface *Langmuir* 2008, *24*, 6154-6158.
12. Thickett, S. C.; Neto, C.; Harris, A. T. Biomimetic Surface Coatings for Atmospheric Water Capture Prepared by Dewetting of Polymer Films *Adv. Mater.* 2011, *23*, 3718-3722.
13. Park, K.-C.; Chhatre, S. S.; Srinivasan, S.; Cohen, R. E.; McKinley, G. H. Optimal design of permeable fiber network structures for fog harvesting. *Langmuir*, Vol. 29, 13269-13277 (2013).
14. Ju, J.; Xiao, K.; Yao, X.; Bai, H.; Jiang, L. Bioinspired Conical Copper Wire with Gradient Wettability for Continuous and Efficient Fog Collection *Adv. Mater.* 2013, *25*, 5937-5942.
15. Heng, X.; Xiang, M.; Lu, Z.; Luo, C. Branched ZnO Wire Structures for Water Collection Inspired by Cacti. *ACS Appl. Mater. Interfaces* 2014**,** *6*, 8032-8041.
16. Heng, X. and Luo, C., Bio-inspired Plate-based Fog Collectors, ACS Applied Materials & Interfaces, Vol. 6(18), pp 16257–16266 (2014).
17. Gischler, C. *The missing link in a production chain, vertical obstacles to catch Camanchaca*. UNESCO, Uruguay, (1991).
18. Holmes, R.; de Dios Rivera, J.; de la Jara, E. Large fog collectors: New strategies for collection efficiency and structural response to wind pressure. *Atmospheric Research*, Vol. 151, 236-249 (2015).
19. de Dios Rivera, J. Aerodynamic collection efficiency of fog water collectors. *Atmospheric Research*, Vol. 102, 335-342 (2011).

20. Schemenauer, R. S.; Cereceda, P. A proposed standard fog collector for use in high-elevation regions. *Journal of Applied Meteorology*, Vol. 33, 1313-1322 (1994).
21. Heerden, J.; Reinhard, D.; Gherezghiher, T.; Olivier, J. Fog as a fresh-water resource: overview and perspectives. *Ambio*, Vol. 41, 221-234 (2012).
22. Cereceda, P.; Larrain, H.; Osses, P.; Farías, M.; Egaña, I. The spatial and temporal variability of fog and its relation to fog oases in the Atacama Desert, Chile. *Atmospheric Research*, Vol. 87, 312-323 (2008).
23. Schemenauer, R. S.; Cereceda, P. A proposed standard fog collector for use in high-elevation regions. *Journal of Applied Meteorology*, Vol. 33, 1313-1322 (1994).
24. Schemenauer, R. S.; Joe, P. I. The collection efficiency of a massive fog collector. *Atmospheric Research*, Vol. 24, 53-69 (1989).
25. Lekouch, I.; Muselli, M.; Kabbachi, B.; Ouazzani, J.; Melnytchouk-Milimouk, I.; Beysens, D. Dew, fog, and rain as supplementary sources of water in south-western Morocco. *Energy*, Vol. 36, 2257-2265 (2011).
26. Garrod, R.; Harris, L.; Schofield, W.; McGettrick, J.; Ward, L.; Teare, D.; Badyal, J. Mimicking a stenocara beetle's back for microcondensation using plasmachemical patterned superhydrophobic-superhydrophilic surfaces. *Langmuir*, Vol. 23, 689-693 (2007).
27. Yu, T. S.; Park, J.; Lim, H.; Breuer, K. S. Fog deposition and accumulation on smooth and textured hydrophobic surfaces. *Langmuir*, Vol. 28, 12771-12778 (2012).
28. Rivera, J. D. D. Aerodynamic Collection Efficiency of Fog Water Collectors. *Atmos. Res.* 2011, 102, 335−342.
29. Langmuir, I.; Blodgett, K. B.: *A Mathematical Investigation of Water Droplet Trajectories. Collected Works of Irving Langmuir*, Pergamon Press: Oxford, U.K., 2004.

30. Kim, G.-T.; Gim, S.-J.; Cho, S.-M.; Koratkar, N.; Oh, I.-K. Wetting-Transparent Graphene Films for Hydrophobic Water-Harvesting Surfaces. *Adv. Mater*. 2014, 26, 5166−5172.
31. Lee, A.; Moon, M.-W.; Lim, H.; Kim, W.-D.; Kim, H.-Y. Water Harvest via Dewing. *Langmuir* 2012, 28, 10183−10191.
32. Heng, X.; Xiang, M. M.; Lu, Z. H.; Luo, C. Branched ZnO wire structures for water collection inspired by Cacti. *ACS Appl. Mater. Interfaces* 2014, 6, 8032.
33. Wang, B. G.; Shi, E. W.; Zhong, W. Z. Understanding and controlling the morphology of ZnO crystallites under hydrothermal conditions. *Cryst. Res. Technol*. 1997, 32 (5), 659.
34. Lafuma, A.; Quéré, D. Superhydrophobic states. Nat. Mater., 2003, 2, 457.
35. Cheng, M. C.; Garra, J. A.; Gadre, A. P.; Nijdam, A. J.; Luo, C.; Paranjape, M.; Currie, J. F.; Schneider, T.; White, R. Dry lease of polymer structures with anti-sticking layer. *J. Vac. Sci. Technol., A* 2004, 22, 837.
36. Wenzel, R. N. Resistance of solid surfaces to wetting by water. *Ind. Eng. Chem.* 1936, 28, 988.
37. Cassie, A. B. D.; Baxter, S. Wettability of porous surfaces. *Trans. Faraday Soc*. 1944, 40, 546.
38. Cheng, Y.-T.; Rodak, D. E.; Angelopoulos, A.; Gacek, T. Microscopic observations of condensation of water on lotus leaves. *Appl. Phys. Lett*. 2005, 87, 194112.
39. Xiang, M.; Wilhelm, A.; Luo, C. Existence and Role of Large Micropillars on a Lotus Leaf. *Langmuir*, 29: 7715-7725, 2013.
40. J.A. Schey, *Introduction to Manufacturing Processes*, 3rd edition, McGraw-Hill College, 1999.

41. Chakraborty, A.; Liu, X.; Luo, C. An Intermediate-layer Lithography Method for Generating Multiple Microstructures Made of Different Conducting Polymers, *Microsystem Technologies*, vol. 13 (8-10), 1175-1184 (2007).

Biographical Information

Mithun Rajaram has received a Bachelor's of Engineering Degree in Mechanical Engineering from Sona College of Technology, Anna University, India in July 2012. During his undergraduate studies, he was a founder of various organizations and he was awarded as successful organizer for organizing multiple National Level Technical Symposiums. His project ideas were very intellectual and his project on "High Speed Projectile Launching" was highly appreciated by professors. His capstone project was "Welding parameters on Weld Penetration" and he assisted multiple projects of his capstone project advisor. He worked as a Mechanical Design Engineer Intern (Pro Bono) for several years and he volunteered himself for mentoring the new team members. He has been a Graduate Student in the Mechanical & Aerospace Engineering Department at UT Arlington since August 2013. He joined Dr. Cheng Luo's group in August 2013 and work with his group on enhancement of fog-collection efficiency of a Raschel mesh using surface coatings and geometric changes. His interests are majorly, product development, project management, medical devices manufacturing and mechanical design.